Journal of Organometallic Chemistry 847 (2017) 132–139

Contents lists available at ScienceDirect

Journal of Organometallic Chemistry

journal homepage: www.elsevier.com/locate/jorganchem

High- and low-spin chelate complexes of iron featuring κ-C,X-$CH_2C_6H_4X$ (X = NMe_2, PMe_2, PPh_2) and κ-C,P-CH_2PMe_2 ligands

Brian P. Jacobs, Peter T. Wolczanski*, Samantha N. MacMillan

Department of Chemistry & Chemical Biology, Baker Laboratory, Cornell University, Ithaca, NY 14853, USA

ARTICLE INFO

Article history:
Received 30 January 2017
Received in revised form
31 March 2017
Accepted 1 April 2017
Available online 5 April 2017

Dedicated to Prof. John Gladysz, for his service to the field of organometallic chemistry, on the occasion of his 65th birthday.

Keywords:
Iron
Chelate
X-ray structure
Oxidative coupling

ABSTRACT

Several C,X-chelate complexes of iron were generated via standard metathetical procedures. Treatment of $FeCl_2$ and L_nFeCl_2 (L = Me_2IPr, n = 1; PMe_3, n = 2) with anionic equivalents o-$LiCH_2C_6H_4NMe_2$, *o*-$LiCH_2C_6H_4PPh_2$, and $LiCH_2PMe_2$ led to the preparation of [Fe(o-$CH_2C_6H_4NMe_2$)]$_2$(κ-μ-CH_2,N-o-$CH_2C_6H_4NMe_2$)$_2$ (**1**, X-ray), [*fac*-Fe(κ-C,P-o-$CH_2C_6H_4PPh_2$)$_3$][Li(TMEDA)$_2$] (**2**, X-ray), (Me_2IPr)Fe($CH_2C_6H_4$-o-NMe_2)$_2$ (**3**-C,N), [(Me_2IPr)$_2$Fe](μ-κ-C,P-CH_2PMe_2)$_2$[Fe(κ-C,P-CH_2PMe_2)$_2$] (**4**, X-ray), and (PMe_3)$_2$Fe(κ-C,P-CH_2PMe_2)$_2$ (**5**). CH-Bond activation of *cis*-(Me_3P)$_4$$FeMe_2$ with *o*-$CH_3C_6H_4PMe_2$ led to the generation of *trans,cis*-(PMe_3)$_2$Fe(κ-C,P-$CH_2C_6H_4$-o-PMe_2)$_2$ (**6**). Exposure of these compounds to [Cp_2Fe][PF_6], a 1e$^-$ oxidant, or AdN_3, here construed as a 2e$^-$ oxidant, led to degradation in all cases, usually with the generation of carbon-carbon coupled ligands as byproducts. The inability of these systems to permit access to higher iron oxidation states is discussed.

1. Introduction

Recent attempts to generate formally Fe(IV) alkylidene complexes capable of conducting olefin metathesis [1–4] have centered on chelate derivatives of iron. Protonation of vinyl-containing chelate compounds generated cationic species [5], and subsequent nucleophilic attack of the imine portion of the chelate led to corresponding neutral derivatives [6]. As Fig. 1 illustrates, while the formal valence bond description of these complexes is Fe(IV), computational evidence supports an Fe(II) carbenium ion and a delocalized imino-vinyl resonance form as being dominant contributors to their electronic structures [7]. A number of other Fe(II) chelate complexes have been prepared as potential precursors to the desired alkylidenes, and these efforts are described herein. The reactivity patterns of the complexes are reconciled according to standard arguments, and through Charge Distribution Via Reporters (CDVR) [8], a new means of assessing the distribution of electron density in molecules.

2. Results

2.1. Ortho-phenyl derived chelates

2.1.1. [Fe(o-$CH_2C_6H_4NMe_2$)]$_2$(κ-μ-CH_2,N-o-$CH_2C_6H_4NMe_2$)$_2$ (**1**)

In order to maximize the donor capacity of the carbon end of a chelate, an amine was considered as its counterpart, since its weak donation should be uncompetitive [9]. The treatment of ferrous chloride with 2 equiv Li(*o*-$CH_2C_6H_4NMe_2$) led to the generation of orange-brown [Fe(o-$CH_2C_6H_4NMe_2$)]$_2$(κ-μ-CH_2,N-o-$CH_2C_6H_4NMe_2$)$_2$ (**1**), as illustrated in Scheme 1. The μ_{eff} of 8.5 μ_B obtained from Evans' method measurements [10] is consistent with two plausible scenarios: 1) two non-interacting iron centers (μ_{SO} = 6.9 μ_B) augmented by significant spin-orbit coupling expected for high spin d^6 centers [11]; 2) two weakly ferromagnetically coupled iron centers (maximum: S_T = 4; μ_{SO} = 8.9 μ_B). The ^{1}H NMR spectrum of the paramagnetic compound was consistent with the structure illustrated, as confirmed by single crystal X-ray crystallography. Clearly, the aryl dialkyl amine donor was not strong enough to support a low spin environment. Attempts to prepare an Fe(III) derivative from 3 equiv of the lithium reagent and $FeCl_3$ afforded **1** and the C-C coupled oxidation product derived from straightforward coupling of the methylene fragments.

* Corresponding author.
E-mail address: ptw2@cornell.edu (P.T. Wolczanski).

http://dx.doi.org/10.1016/j.jorganchem.2017.04.001
0022-328X/

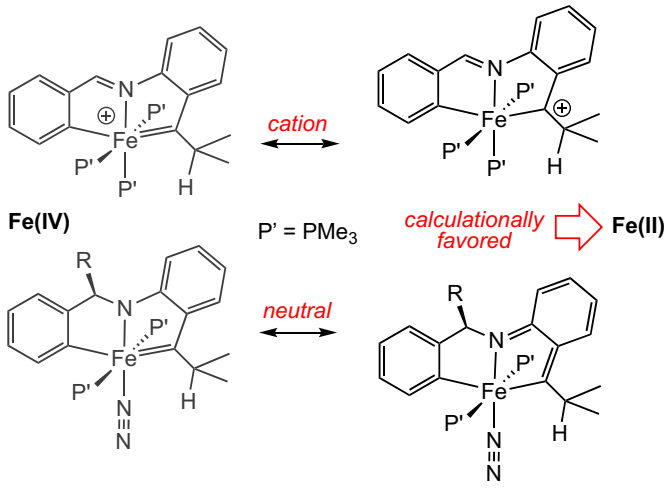

Fig. 1. Formal Fe(IV) cationic and neutral alkylidene chelates are computed to have a significant contribution from Fe(II) resonance forms.

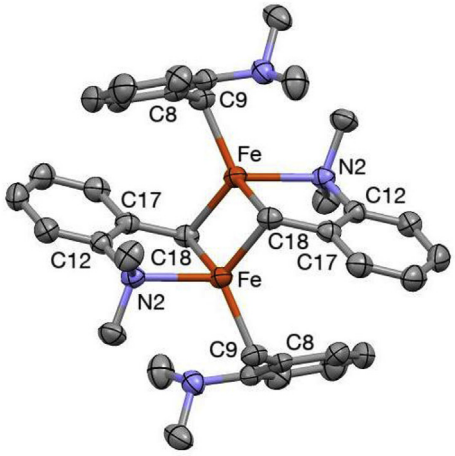

Fig. 2. Molecular view of [{$Me_2N(o\text{-}C_6H_4)CH_2$}Fe(κ-μ-$CH_2$,N-o-$CH_2C_6H_4NMe_2$)] (**1**). Selected interatomic distances (Å) and angles (°): Fe-Fe, 2.5930(5); Fe-C9, 2.0650(19); Fe-μ-C18, 2.136(2), 2.221(2); Fe-N2, 2.2028(16); C18-C18, 2.593(3); C9-Fe-μ-C18, 113.46(8), 124.60(8); C9-Fe-N2, 112.89(7); N2-Fe-μ-C18, 79.70(6), 112.25(7); μ-C18-Fe-μ-C18, 106.98(6); Fe-μ-C18-Fe, 73.01(6) Fe-C9-C8, 106.62(13); Fe-μ-C18-C17, 108.74(12), 109.23(13); Fe-N2-C12, 111.68(11).

2.1.2. *Structure of [Fe(o-$CH_2C_6H_4NMe_2$)]$_2$(κ-μ-CH_2,N-o-$CH_2C_6H_4NMe_2$)$_2$ (**1**)*

Fig. 2 illustrates a view of centrosymmetric dimer **1**, and its caption lists pertinent metric parameters. The structure is related to [Mn(o-$CH_2C_6H_4NMe_2$)](κ-μ-CH_2,N-o-$CH_2C_6H_4NMe_2$)$_2$[Mn(κ^2-o-$CH_2C_6H_4NMe_2$)], which contains one manganese center with a terminal benzyl, and one with an additional chelating unit [12,13]. Each iron center is a distorted tetrahedron, with one terminal $CH_2C_6H_4$-o-NMe_2 ligand, an amine, and two bridging benzyl ligands, easily the most interesting feature of the molecule. The Fe_2(μ-CH_2Ar)$_2$ core is planar, with ∠(μ-C18)-Fe-(μ-C18) = 106.98(6)°, and/Fe-μ-C18-Fe = 73.01(6)°, while the κ-μ-CH_2,N-o-$CH_2C_6H_4NMe_2$ chelate links the μ-CH_2Ar bridge to iron above and below the diamond core. The terminal benzyl carbon makes 113.46(8) and 124.60(8)° angles with the bridging benzyl carbons, but the amine possesses dissimilar corresponding angles of 112.25(7)° and 79.70(6)°, the latter acute due to chelation. The terminal iron-carbon and -nitrogen bond distances are 2.0650(19) and 2.2028(16) Å, respectively, which are typical values for high spin Fe(II) [14,15]. The bridges are slightly asymmetric, with d(Fe-μ-C18) = 2.136(2) and 2.221(2) Å, the lengthier distance affiliated with its chelating amine. While the CH bonds of the benzyls might be construed as agostic, ranging from 2.00(2)-3.02(2) Å, these distances are likely consequence of the benzyl geometry (/Fe-(μ-C18)-C17 = 108.74(12), 109.23(13)) rather than any significant interaction with the high spin ferrous center.

2.1.3. *[fac-Fe(κ-C,P-o-$CH_2C_6H_4PPh_2$)$_3$][Li(TMEDA)] (**2**)*

The high spin nature of the C,N-based chelates prompted a switch to phosphorus, and treatment of $FeCl_2$ with 3 equiv $PPh_2C_6H_4$-o-CH_2Li(TMEDA) [16] afforded microcrystalline red [*fac*-Fe(κ-C,P-o-$CH_2C_6H_4PPh_2$)$_3$][Li(TMEDA)$_2$] (**2**) in 73% yield, as illustrated in Scheme 1. The ^{1}H NMR spectrum of **2** revealed broad resonances in positions indicative of a diamagnetic complex, consistent with a stronger field imparted by the C,P-bound chelates, but determination of the geometry depended on X-ray crystallography.

2.1.4. *Structure of [fac-Fe(κ-C,P-o-$CH_2C_6H_4PPh_2$)$_3$][Li(TMEDA)] (**2**)*

The *fac*-geometry of [*fac*-Fe(κ-C,P-o-$CH_2C_6H_4PPh_2$)$_3$][Li(TMEDA)$_2$] (**2**) was confirmed by an X-ray structural study, and the pseudo-octahedral, C_3-symmetric ferrous anion is illustrated in Fig. 3, which is accompanied by metric parameters listed in its

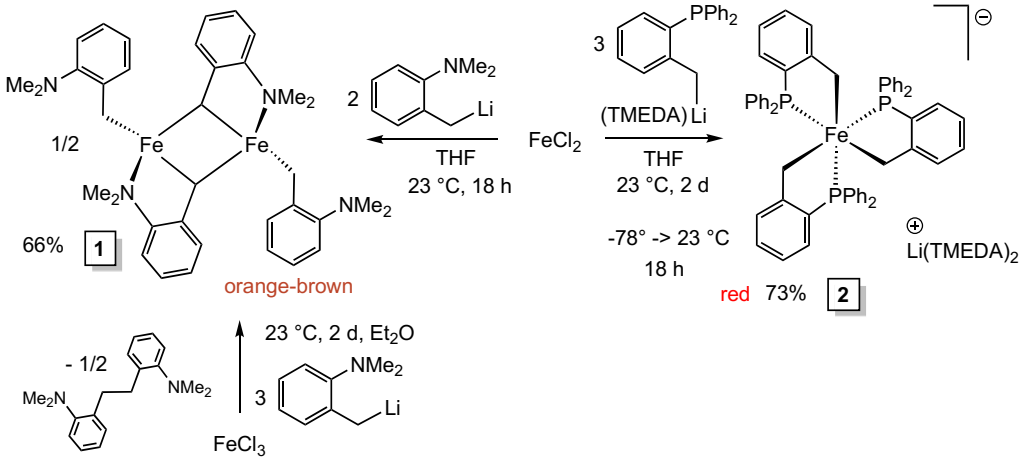

Scheme 1. Syntheses of dimer [Fe(o-$CH_2C_6H_4NMe_2$)]$_2$(κ-μ-CH_2,N-o-$CH_2C_6H_4NMe_2$)$_2$ (**1**) and the pseudo-octahedral anionic complex [*fac*-Fe(κ-C,P-o-$CH_2C_6H_4PPh_2$)$_3$][Li(TMEDA)$_2$] (**2**).

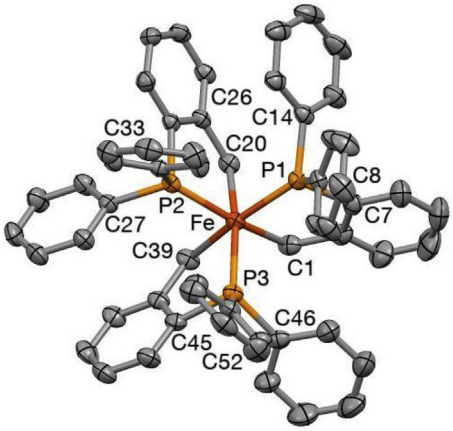

Fig. 3. Molecular view of the anion of [*fac*-Fe(κ-C,P-*o*-$CH_2C_6H_4PPh_2)_3$][Li(TMEDA)$_2$] (**2**). Selected interatomic distances (Å) and angles (°): Fe-C1, 2.1028(18); Fe-C20, 2.0976(18); Fe-C39, 2.1160(18); Fe-P1, 2.2170(5); Fe-P2, 2.2278(5); Fe-P3, 2.2198(5); PC_{ipso}(ave), 1.854(16); C1-Fe-C20, 82.84(7); C1-Fe-C39, 83.65(8); C20-Fe-C39, 85.13(7); P1-Fe-P2, 102.391(19); P1-Fe-P3, 106.74(2); P2-Fe-P3, 101.81(2); C1-Fe-P1, 82.34(5); C1-Fe-P2, 163.59(6); C1-Fe-P3, 91.64(6); C20-Fe-P1, 87.22(5); C20-Fe-P2, 81.72(5), C20-Fe-P3, 164.24(5); C39-Fe-P1, 164.77(6); C39-Fe-P2, 89.53(6); C39-Fe-P3, 79.58(5).

averaging 81.2(14)° are significantly smaller than the corresponding interchelate C-Fe-P angles of 89.5(22)° (ave), and C-Fe-C angles that average 83.8(12)° are considerable less than the interphosphine P-Fe-P angles of 103.6(27)° (ave), presumably due to steric interactions. *Trans*-C-Fe-P angles of 164.2(6)° show that the deviation from ideal pseudo-octahedral symmetry is moderate.

2.1.5. Oxidations of *o*-phenyl derived chelate derivatives

As a means of generating Fe=CHX components within a chelate, sequential oxidations of Fe(II) followed by deprotonation were considered as a route. In a series of NMR tube scale reactions in C_6D_6 or THF-d_8 and small pot reactions, [Fe(o-$CH_2C_6H_4NMe_2$)](κ-μ-CH_2,N-o-$CH_2C_6H_4NMe_2)_2$ (**1**) was subjected to a variety of oxidants with disappointing results, as Scheme 2 illustrates. While it was expected that Fe(III) intermediates would be isolable, this proved to be unfounded, as treatment of **1** with stoichiometric oxidants generally afforded *o*-NMe_2-$C_6H_4CH_2CH_2C_6H_4$-*o*-NMe_2, an oxidatively coupled product derived from the chelate. Trace amine- and imine-products, presumably derived from adamantyl nitrene insertion into the iron-benzyl bonds, are also observed in the oxidation of **1** by AdN_3. The metal products were not determined in these reactions. A corresponding oxidation of [*fac*-Fe(κ-C,P-o-

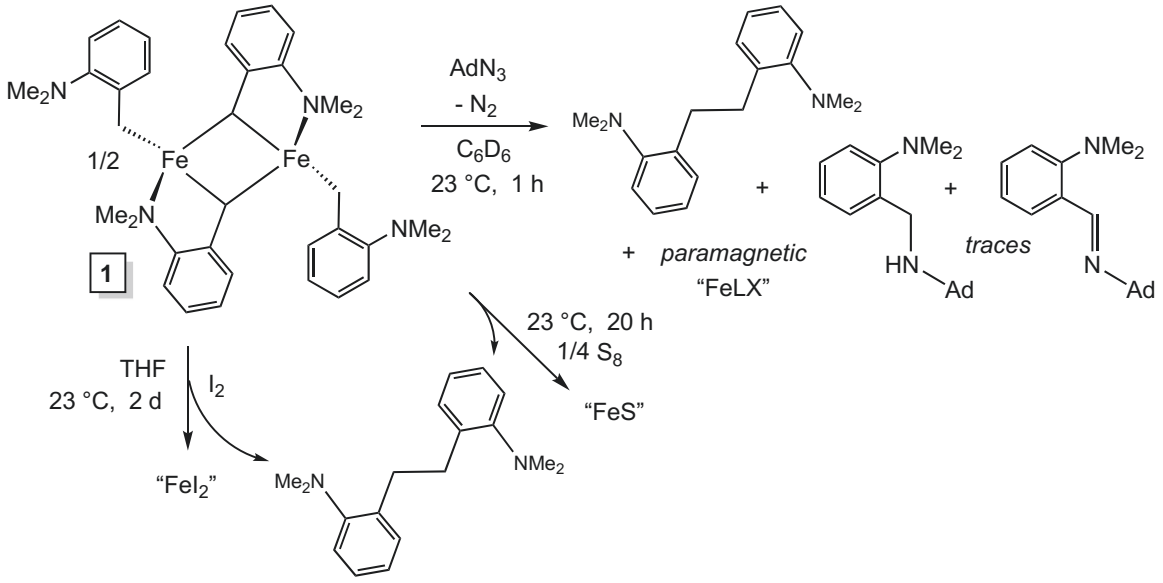

Scheme 2. Oxidative degradations of [Fe(o-$CH_2C_6H_4NMe_2$)]$_2$(κ-μ-CH_2,N-o-$CH_2C_6H_4NMe_2)_2$ (**1**) revealing nitrene insertion and C-C coupling products.

caption. The set of bond lengths appears to reflect the anionic character of the ferrous center, as the iron-carbon (benzyl) bonds average a rather lengthy 2.106(10) Å, while the d(Fe-P) average 2.222(6) Å, a value that is normal [5–7]. Chelate bite angles

$CH_2C_6H_4PPh_2)_3$][Li(TMEDA)] (**2**) with $[Cp_2Fe]PF_6$ afforded the related coupled product, *o*-PPh_2-$C_6H_4CH_2CH_2C_6H_4$-*o*-PPh_2 (eq (1)) At this point, these chelates were abandoned as potential Fe(IV) alkylidene precursors in favor of mixed ligand species.

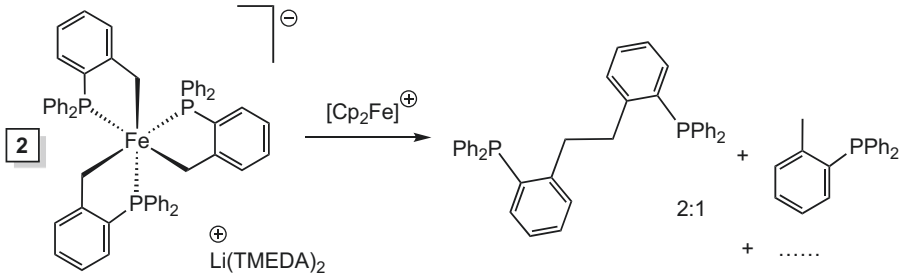

(1)

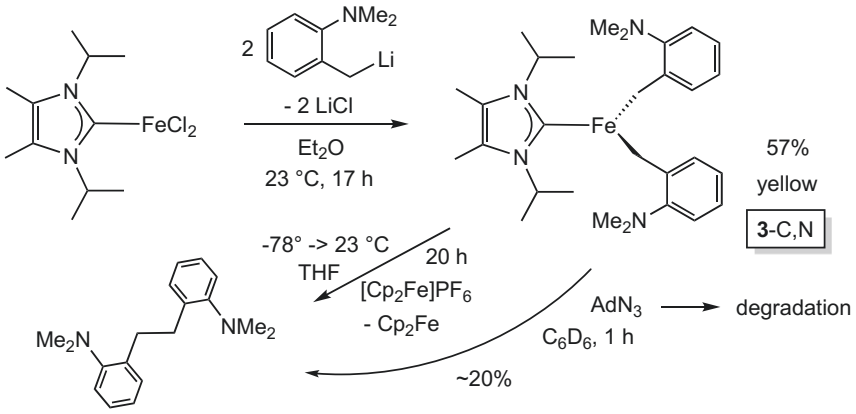

Scheme 3. Synthesis of $(Me_2IPr)Fe(CH_2C_6H_4\text{-}o\text{-}NMe_2)_2$ (**3**-C,N) and C-C coupling upon oxidation.

2.2. Chelate derivatives supported by ancillary ligands

2.2.1. Synthesis and reactivity of $(Me_2IPr)Fe(CH_2C_6H_4\text{-}o\text{-}NMe_2)_2$ (**3**)

Since the aforementioned chelates were not found to support higher oxidation states, chelates in combination with ancillary ligands were utilized. The N-heterocyclic carbene precursor, $(Me_2IPr)FeCl_2$ [17,18], whose aggregation state is unknown, was generated via stoichiometric mixing of Me_2IPr and $FeCl_2$ in THF and used without isolation or further purification. As Scheme 3 indicates, addition of 2 equiv $Li(o\text{-}CH_2C_6H_4NMe_2)$ to $(Me_2IPr)FeCl_2$ provided yellow microcrystalline $(Me_2IPr)Fe(CH_2C_6H_4\text{-}o\text{-}NMe_2)_2$ (**3**-C,N) in 57% yield. Evans' method measurements [10] indicated a high spin environment ($\mu_{eff} = 5.2\ \mu_B$), consistent with a low coordinate $S = 2$ ferrous center [11]. Amine coordination leading to 4- or 5-coordinate species cannot be ruled out, although precedent [18,19] suggests that the complex is 3-coordinate, given the weak donor capacity of the amine. A one-electron oxidation attempt with ferricinium, and a two-electron oxidation attempt with adamantyl azide, each generated the coupled degradation product, $o\text{-}NMe_2\text{-}C_6H_4CH_2CH_2C_6H_4\text{-}o\text{-}NMe_2$.

2.2.2. Synthesis $[(Me_2IPr)_2Fe](\mu\text{-}\kappa\text{-}C,P\text{-}CH_2PMe_2)_2[Fe(\kappa\text{-}C,P\text{-}CH_2PMe_2)_2]$ (**4**)

A switch to β-phosphine alkyls was considered, as these ligands had some intriguing possibilities as mono-and bidentate ligands [20,21]. Deprotonation of Me_3P is readily effected to produce $LiCH_2PMe_2$ [22], and exposure of $(Me_2IPr)FeCl_2$, with 2 equiv of the reagent produced an orange, microcrystalline product. Evans' method measurements [10] were lower than anticipated for $(Me_2IPr)Fe(\kappa\text{-}C,P\text{-}CH_2PMe_2)_2$ (**3**-C,P), prompting an X-ray structural analysis of the complex. If **3**-C,P was initially generated, a ligand redistribution occurred to give the final product, the binuclear complex $[(Me_2IPr)_2Fe](\mu\text{-}\kappa\text{-}C,P\text{-}CH_2PMe_2)_2[Fe(\kappa\text{-}C,P\text{-}CH_2PMe_2)_2]$ (**4**), as shown in Scheme 4. The μ_{eff} of 5.0(3) μ_B is consistent with a single high spin iron(II) center ($\mu_{SO} = 4.9\ \mu_B$) [11]. Oxidation studies were not pursued, given the structural findings, but redistribution suggested a phosphine derivative would possibly be intriguing.

2.2.3. Structure of $[(Me_2IPr)_2Fe](\mu\text{-}\kappa\text{-}C,P\text{-}CH_2PMe_2)_2[Fe(\kappa\text{-}C,P\text{-}CH_2PMe_2)_2]$ (**4**)

A molecular view of the binuclear complex $[(Me_2IPr)_2Fe](\mu\text{-}\kappa\text{-}C,P\text{-}CH_2PMe_2)_2[Fe(\kappa\text{-}C,P\text{-}CH_2PMe_2)_2]$ (**4**) is given in Fig. 4, and critical metric parameters are provided in its caption. The four-coordinate component is a fairly regular tetrahedron, with core angles averaging 109.6(52), and bond distances (d(FeC(P)) = 2.113(2) Å (ave), d(FeC(NN)) = 2.169(6) Å (ave)) consistent with

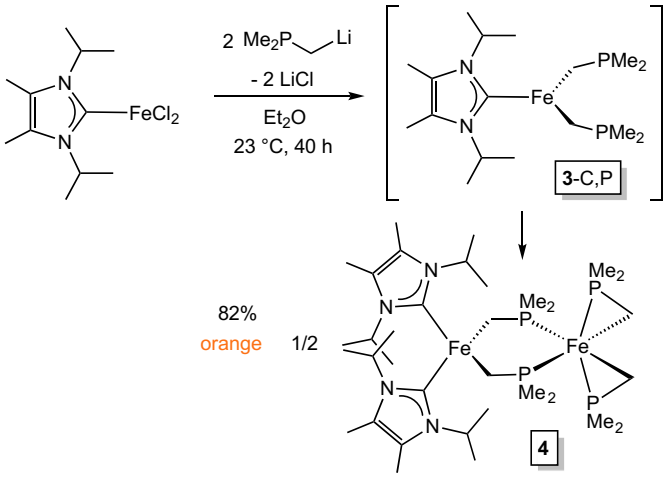

Scheme 4. Attempted synthesis of $(Me_2IPr)Fe(\kappa\text{-}C,P\text{-}CH_2PMe_2)_2$ (**3**-C,P), and the isolated redistribution product, $[(Me_2IPr)_2Fe](\mu\text{-}\kappa\text{-}C,P\text{-}CH_2PMe_2)_2[Fe(\kappa\text{-}C,P\text{-}CH_2PMe_2)_2]$ (**4**).

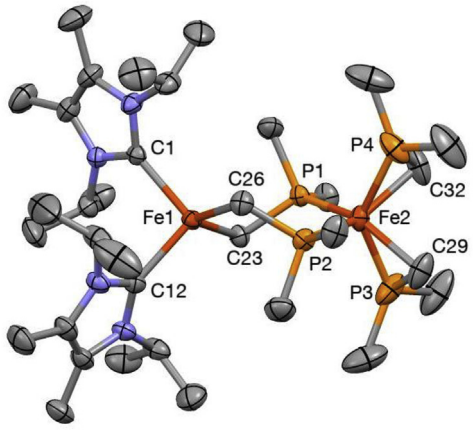

Fig. 4. Molecular view of $[(Me_2IPr)_2Fe](\mu\text{-}\kappa\text{-}C,P\text{-}CH_2PMe_2)_2[Fe(\kappa\text{-}C,P\text{-}CH_2PMe_2)_2]$ (**4**). Selected interatomic distances (Å) and angles (°): Fe1-C1, 2.173(2); Fe1-C12, 2.165(2); Fe1-C23, 2.114(2); Fe1-C26, 2.111(2); Fe2-P1, 2.1842(6); Fe2-P2, 2.1917(6); Fe2-P3, 2.1055(7); Fe2-P4, 2.1090(7); Fe2-C29, 2.111(2); Fe2-C32, 2.117(2); C29-P3, 1.739(3); C32-P4, 1.738(3); C23-P1, 1.804(2); C26-P2, 1.805(2); C1-Fe1-C12, 99.67(7); C1-Fe1-C23, 109.33(8); C1-Fe1-C26, 113.24(8); C12-Fe1-C23, 112.67(8); C12-Fe1-C26, 113.24(8); C23-Fe1-C26, 109.24(8); P1-Fe2-P2, 97.59(2); P1-Fe2-P3, 100.92(3); P1-Fe2-P4, 108.75(3); P2-Fe2-P3, 108.39(3); P2-Fe2-P4, 101.32(3); P3-Fe2-P4, 134.32(3); C29-Fe2-P3, 48.72(8); C29-Fe2-P1, 149.62(8); C29-Fe2-P2, 94.46(8); C29-Fe2-P4, 95.97(9); C32-Fe2-P4, 48.56(8); C32-Fe2-P1, 93.35(8); C32-Fe2-P2, 149.88(8); C32-Fe2-P3, 96.86(9); Fe2-C29-P3, 65.48(8); Fe2-P3-C29, 65.80(9); Fe2-C32-P4, 65.48(8), Fe2-P4-C32, 65.97(9).

a high spin ferrous center. The six-coordinate ferrous center is highly irregular, and is actually close to being tetrahedral if each η^2-CH_2PMe_2 ligand is considered as a unit. The CH_2 groups are 149.67(8)° and 148.88(8)° from the phosphorus atoms in the bridging μ-κ-C,P-CH_2PMe_2 ligands. The phosphines almost comprise another tetrahedron, with only the P3-Fe2-P4 angle of 134.32(3)° significantly larger than the 103.4(49)° average of the remaining five P-Fe-P angles. The d(Fe2-C) of 2.114(4) Å (ave) are somewhat long (~0.15 Å) for a low spin Fe(II) center [5–7], but in combination with the phosphines, render the pseudo-octahedral center diamagnetic. It is interesting that the iron carbon distances of the bridging alkyl are essentially identical to those of the η^2-CH_2PMe_2 ligand.

*2.2.4. Synthesis and reactivity of $(PMe_3)_2Fe(\kappa$-C,P-$CH_2PMe_2)_2$ (**5**)*

The addition of 2 equiv $LiCH_2PMe_2$ to $(Me_3P)_2FeCl_2$ [23] led to the isolation, in 24% yield, of a sticky brown diamagnetic material formulated as $(PMe_3)_2Fe(\kappa$-C,P-$CH_2PMe_2)_2$ (**5**), as indicated in eq (2). Its ^1H NMR spectrum was consistent with a structure containing a mirror plane, and its two ^{31}P resonances were indicative of bound PMe_3, and bidentate κ-C,P-CH_2PMe_2 ligands. In addition, **5** has essentially the same coordination environment as the six-coordinate portion of $[(Me_2IPr)_2Fe](\mu$-κ-C,P-$CH_2PMe_2)_2[Fe(\kappa$-C,P-$CH_2PMe_2)_2]$ (**4**), hence the μ_{eff} for **4** is probably indicative of a high spin tetrahedral center and a low spin ($S = 0$) pseudo-octahedral ferrous site.

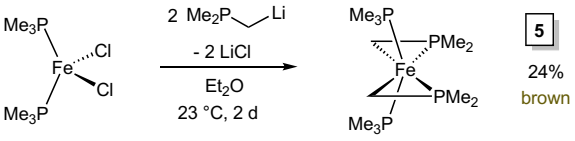

(2)

The stability of the pseudo-octahedral $(PMe_3)_2Fe(\kappa$-C,P-$CH_2PMe_2)_2$ (**5**) was significantly greater than the previously assessed lower coordinate species. Upon exposure to AdN_3 for prolonged periods, **5** was stable, and thermolysis of the reaction mixture up to 90 °C led only to azide degradation, but no reaction. Related thermolyses in the presence of *cis*-2-pentene gave no indication that decomposition products, such as alkylidenes resulting from α-PMe_2 migration, might mediate olefin metathesis.

diamagnetic as expected. Unfortunately, attempts to oxidize **6** failed to elicit stable compounds. For example, treatment of **6** with $[Cp_2Fe][PF_6]$ afforded the C-C coupled oxidation product *o*-PMe_2-$C_6H_4CH_2CH_2C_6H_4$-*o*-PMe_2 and Cp_2Fe, and no tractable metal-containing species was evident.

3. Discussion

3.1. Chelate complexes of Iron(II)

A variety of C,X-chelate complexes of iron(II) have been prepared, mostly through metathetical reactions involving lithium anions and ferrous chloride or its derivatives. In general, this was a satisfactory approach aside from $(PMe_3)_2Fe(\kappa$-C,P-$CH_2PMe_2)_2$ (**5**), and in this case the high solubility of the complex, and its oily/waxy consistency were the probable cause of the low yield (~24%). The phosphine-carbon based chelates enforce a low spin environment because of their significant field strength, and [*fac*-Fe(κ-C,P-*o*-$CH_2C_6H_4PPh_2)_3$][Li (TMEDA)$_2$] (**2**), the pseudo-octahedral "half" of $[(Me_2IPr)_2Fe](\mu$-κ-C,P-$CH_2PMe_2)_2[Fe(\kappa$-C,P-$CH_2PMe_2)_2]$ (**4**), $(PMe_3)_2Fe(\kappa$-C,P-$CH_2PMe_2)_2$ (**5**), and *trans,cis*-$(PMe_3)_2Fe(\kappa$-C,P-$CH_2C_6H_4$-*o*-$PMe_2)_2$ (**6**) are all diamagnetic as a consequence. As a corollary, the field strength of the C,N-chelates is relatively weak, and $[Fe(o\text{-}CH_2C_6H_4NMe_2)]_2(\kappa\text{-}\mu\text{-}CH_2$,N-*o*-$CH_2C_6H_4NMe_2)_2$ (**1**), and $(Me_2IPr)Fe(CH_2C_6H_4$-*o*-$NMe_2)_2$ (**4**-C,N) are all high spin.

3.2. Oxidative degradation of Iron(II)

The sequential oxidation of iron(II) chelates and deprotonation of the chelate Fe-CH_2- connection was considered as a means to generate Fe=CHX functionality, but none of the compounds survive either $1e^-$ oxidants (i.e., $[Cp_2Fe][PF_6]$) or chemical agents that serve as $2e^-$ oxidants, here typically represented by AdN_3. The products of these reactions were mostly C-C coupled species derived from the carbon arms of the chelates. While related chelates have been able to accommodate these oxidations [5–7,25,26], at least to Fe(III) and to configurations that appear Fe(IV) but are more realistically Fe(II) (Fig. 1), these species did not show this capability, although $(PMe_3)_2Fe(\kappa$-C,P-$CH_2PMe_2)_2$ (**5**) was remarkably stable and resistant to oxidation. One rationalization is that the Fe-CH_2X fragments constructed all had electron-withdrawing groups as X, and none of the chelates were able to stabilize a less electron-rich center than Fe(II).

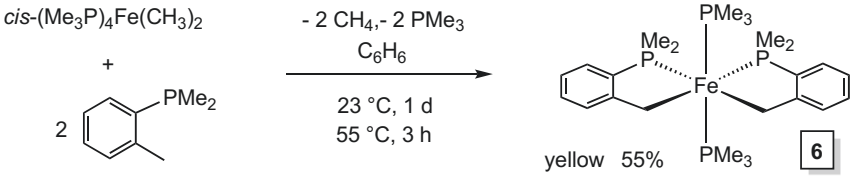

(3)

*2.2.5. Synthesis and reactivity of cis,trans-$(PMe_3)_2Fe(\kappa$-C,P-$CH_2C_6H_4$-*o*-$PMe_2)_2$ (**6**)*

Instead of using salt metathesis to install the κ-C,P-$CH_2C_6H_4$-*o*-PMe_2 ligand akin to Scheme 1, a C-H bond activation methodology was employed. Kharsch's *cis*-$(Me_3P)_4FeMe_2$ complex [24] is known to react with activated CH bonds to expel methane [25–28], so it was treated with *o*-CH_3-$C_6H_4PMe_2$ for 1 day at 23 °C, then heated at 55 °C for 3 h to produce yellow *trans,cis*-$(PMe_3)_2Fe(\kappa$-C,P-$CH_2C_6H_4$-*o*-$PMe_2)_2$ (**6**) in 55% yield, as shown in eq (3). The switch from PPh_2 to PMe_2 should induce a stronger field at iron, and compound **6** is

These laboratories recently conceptualized Charge Distribution Via Reporters (CDVR) [8], a means of numerically assessing the distribution of electron density. In this methodology, the charge on iron is fixed at $\mathbf{c}_{Fe} = +2.0$, and the charge on each CH_2 groups is likely to be $\mathbf{c}_R \leq -0.65$. As a consequence, the phosphines in $(PMe_3)_2Fe(\kappa$-C,P-$CH_2PMe_2)_2$ (**5**), and *trans,cis*-$(PMe_3)_2Fe(\kappa$-C,P-$CH_2C_6H_4$-*o*-$PMe_2)_2$ (**6**) (for example), compensate the charge on iron with ~ −0.7 units of charge in the Fe(II) species. When oxidized by one electron, all the ligands must be able to accommodate the increase in charge by summing to −1.0 charge units.

Trialkylphosphines are flexible to ~ +0.10, but the aryl-phosphines in this study are considerably more electron-withdrawing, and the putative Fe(III) species are at best on the cusp of stability. Carbon-carbon bond formation via reductive elimination, and redistribution of product iron species appear to be the natural consequence.

4. Conclusions

A series of C,X-chelate complexes of iron have been prepared, containing amines (X = NMe_2) and phosphines (X = PMe_2, PPh_2) but neither the weak field amine or strong field phosphine derivatives have proven to be stable with respect to oxidation. As a consequence, less electron-withdrawing alkyls and ancillary ligands are now being considered.

5. Experimental

5.1. General considerations

All manipulations were performed using either glovebox or high vacuum line techniques under inert atmosphere (Ar), unless stated otherwise. All glassware was oven dried at 180 °C. THF and ether were distilled under nitrogen from purple sodium benzophenone ketyl and vacuum transferred from the same prior to use. Hydrocarbon solvents were treated in the same manner with the addition of 1–2 mL/L tetraglyme. Tetramethylethylenediamine (tmeda) was stirred over sodium/benzophenone, then vacuum transferred to a fresh flask containing charged with sodium and benzophenone. Benzene-d_6 was dried over sodium, vacuum transferred and stored over sodium. THF-d_8 was dried over sodium, and vacuum transferred from sodium benzophenone ketyl prior to use. Chloroform-d_1 (Cambridge Isotope Laboratories) was used as received. $LiCH_2C_6H_4$-*o*-NMe_2 [9,29], $LiCH_2PMe_2$ [22], 1,3-diisopropyl-4,5-dimethyl-1*H*-imidazol-3-ium-2-ide (Me_2IPr) [17], $CH_3C_6H_4$-*o*-PPh_2 [16], $FeCl_2(PMe_3)_2$ [23], and *cis*-$Me_2Fe(PMe_3)_4$ [24] were prepared according to literature procedures. (Me_2IPr)$FeCl_2$ [18] was prepared by stirring $FeCl_2$ with 1 eq. Me_2IPr in THF for 1 h (until solids dissolve completely) at 23 °C, followed by evaporation of the solvent under vacuum. Organic products were determined by NMR spectral analysis and Mass spectrometry (DART). All other chemicals were commercially available and used as received.

NMR spectra were obtained using Inova 400 MHz, 500 MHz and 600 MHz spectrometers. Chemical shifts are reported relative to benzene-d_6 (^{1}H δ 7.16; ^{13}C{^{1}H} δ 128.39), THF-d_8 (^{1}H δ 3.58; ^{13}C{^{1}H} δ 67.57) and chloroform-d_1 (^{1}H δ 7.26; ^{13}C{^{1}H} δ 77.16). Accurate mass data were acquired on an Exactive Orbitrap mass spectrometer (Thermo Scientific) using a DART (IonSense Inc., Saugus, MA) ion source in positive ion mode using helium for DART ionization, while software affiliated with the spectrometer was used to calculate the molecular weight. Solution magnetic measurements were conducted via Evans' method in C_6D_6 or THF-d_8 [10]. Analytical data were obtained from the CENTC Elemental Analysis Facility at the University of Rochester, funded by NSF CHE-0650456.

5.2. Procedures

5.2.1. $Li(tmeda)CH_2C_6H_4$-*o*-PPh_2

This procedure is in accordance with César *et. al.* [16]. Addition of ^{n}BuLi in hexanes (10.4 mmol, 1.60 M) to a 100-mL flask charged with $CH_3C_6H_4$-*o*-PPh_2 (2.40 g, 8.69 mmol), 30 mL ether, 3 mL pentane and 1.60 mL TMEDA resulted in precipitation of orange microcrystals, and the mixture was stirred at 23 °C for 18 h. Filtration of the precipitate yielded the title compound as orange crystals (2.757 g, 80%). ^{1}H NMR (C_6D_6): δ 1.66 (4H, s), 1.83 (12H, s), 6.23 (1H, t, 7 Hz), 6.77 (1H, t, 7 Hz), 7.03 (1H, m), 7.11 (3H, m), 7.18 (4H, m), 7.60 (4H, t, 7 Hz). ^{13}C NMR (C_6D_6): δ 45.10, 56.26, 107.84, 120.28, 128.51, 128.55, 128.63, 129.36, 133.34, 134.66, 134.86, 137.25, 168.69. ^{31}P NMR (C_6D_6): δ −15.52 (s).

5.2.2. $CH_3C_6H_4$-*o*-PMe_2

This procedure is a modification of the Wright *et. al.* procedure [30]. A 3-neck 100-mL flask was fit with a glass stopper, a solid addition glass finger charged with $ZnCl_2$ (1.912 g, 14.03 mmol), and a 180° Schlenk adapter. The glassware was degassed, and 16 mL THF was added via vacuum transfer to the flask. *o*-Bromotoluene (2.000 g, 11.69 mmol) was added to the flask, which was then cooled to −78 °C. Addition of ^{n}BuLi in hexanes (12.8 mmol, 1.60 M) resulted in a cloudy suspension, which was stirred for 15 min at −78 °C. An additional 16 mL THF was added via vacuum transfer, the $ZnCl_2$ solid was added to the suspension at −78 °C, and the mixture was stirred for 2 h PCl_3 (1.2 mL, 14 mmol) was added via vacuum transfer, and the mixture was allowed to warm slowly to 23 °C with stirring over 18 h. The solution was cooled to 0 °C and the volatiles removed *in vacuo*, yielding a colorless oil. 30 mL ether was transferred under vacuum to the flask. With the flask cooled to −78 °C, 32.2 mL of MeLi in ether (51.5 mmol, 1.60 M) was added, and the mixture became translucent yellow with a colorless precipitate. The mixture was allowed to warm slowly over 20 h. The flask was cooled with to 0 °C, and 30 mL ice cold water was slowly added to the flask, generating small amounts of gas evolution until no effervescence was observed. The flask was removed from the adapter, the mixture added to a 250-mL Erlenmeyer flask and diluted with 50 mL ether. The mixture was filtered, and the organic layer was separated from the aqueous layer. The aqueous layer was extracted with 2 × 25 mL portions of ether, the combined organic extracts dried over $MgSO_4$ and filtered. Removal of the solvent *in vacuo* at 0 °C yielded a yellow oil (1.421 g, 79%), which was stored under a nitrogen in a glovebox. Its purity was estimated at ~93% based on its ^{31}P NMR spectrum. ^{1}H NMR (C_6D_6): δ 1.03 (6H, d, 4 Hz), 2.48 (3H, s), 7.01 (1H, m), 7.09 (2H, m), 7.24 (1H, m). ^{13}C NMR (C_6D_6): δ 13.57 (d, 14 Hz), 20.04 (d, 23 Hz), 126.38, 128.36, 128.60 (d, 1 Hz), 130.26 (d, 4 Hz), 168.68. ^{31}P NMR (C_6D_6): δ −58.05.

5.2.3. [Fe(*o*-$CH_2C_6H_4NMe_2$)]$_2$(κ-μ-CH_2,N-*o*-$CH_2C_6H_4NMe_2$)$_2$ (**1**)

a. To a 50-mL flask charged with $FeCl_2$ (225 mg, 1.78 mmol) and $LiCH_2C_6H_4$-*o*-NMe_2 (500 mg, 3.54 mmol) was added 25 mL THF via vacuum transfer at −78 °C, resulting in a dark-orange solution. The solution was allowed to warm slowly with stirring for 18 h. The volatiles were removed, and the residue was taken up in 15 mL THF and filtered through dried Celite. Removal of the solvent *in vacuo* followed by washing the residue with hexanes (3 × 15 mL) resulted in brown-orange microcrystals (380 mg, 66%), with a purity of ~94% based on NMR spectroscopy. *b.* To a 25-mL flask charged with $FeCl_3$ (115 mg, 0.709 mmol) and $LiCH_2C_6H_4$-*o*-NMe_2 (300 mg, 2.13 mmol) was added 10 mL ether via vacuum transfer at −78 °C. The light orange suspension was allowed to warm slowly with stirring for 2 d, resulting in a dark red-orange solution at 21 °C. Evaporation of the volatiles, and washing the residue with pentane (3 × 10 mL) resulted in brown microcrystals of **1**. Crystals suitable for X-ray diffraction were obtained via slow evaporation of a concentrated ether solution. ^{1}H NMR (C_6D_6): δ −18.41 (4H), 2.61 (4H), 17.53 (4H), 18.44 (4H), 89.07 (12H). μ_{eff} (Evans) = 8.5 μ_B.

5.2.4. [*fac*-Fe(κ-C,P-*o*-$CH_2C_6H_4PPh_2$)$_3$][Li(TMEDA)] (**2**)

To a 25-mL flask charged with $FeCl_2$ (43 mg, 0.34 mmol) and Li(tmeda)$CH_2C_6H_4$-*o*-PPh_2 (400 mg, 1.00 mmol) was added 15 mL THF via vacuum transfer at −78 °C. The yellow suspension was allowed to warm slowly to 23 °C and stirred for 2 d, during which time the solution turned a dark-red. The volatiles were removed, and the residue taken up in 10 mL THF and filtered through dried

Celite. The THF was removed, and the residue was washed with hexanes (3 × 10 mL), and the red suspension filtered in hexanes to afford a red powder (275 mg, 73%). Crystals suitable for X-ray diffraction were obtained via letting a concentrated C_6D_6 solution stand for 12 h at 23 °C. ^{1}H NMR (C_6D_6): δ 1.41 (4H, br s), 1.64–1.70 (24H, br "s"), 2.42 (1H, s), 3.44 (1H, s), 3.55 (4H, br s), 6.76 (2H, br s), 6.79–6.94 (14H, m), 7.00 (4H, m), 7.03–7.05 (10H, m), 7.06 (1H, t, 7 Hz), 7.10 (1H, dd, 4 7 and 4 Hz), 7.14 (1H, br s), 7.23–7.29 (3H, m), 7.37 (5H, m), 7.94 (4H, m). ^{31}P NMR (C_6D_6): δ −13.37 (1P), −15.71 (2P).

5.2.5. *(Me$_2$IPr)Fe(CH$_2$C$_6$H$_4$-o-NMe$_2$)$_2$ (**3**-C,N)*

To a 25-mL flask charged with (Me$_2$IPr)FeCl$_2$ (218 mg, 0.710 mmol) and LiCH$_2$C$_6$H$_4$-*o*-NMe$_2$ (200 mg, 1.42 mmol) was added 10 mL ether via vacuum transfer at −78 °C. The yellow suspension did not change color, and was allowed to slowly warm with stirring for 17 h. At 23 °C, the solution turned brown-orange with colorless precipitate, and was filtered. The ether solution was concentrated and cooled to −78 °C for 15 min. The solution was filtered, and concentrated to afford yellow microcrystals (202 mg, 57%), whose purity was assessed at ~97% based on NMR spectroscopy. ^{1}H NMR (C_6D_6): δ −27.95 (2H), −13.69 (2H), −9.21 (6H), 16.14 (12H), 25.57 (2H), 38.88 (2H), 40.45 (12H). μ_{eff} (Evans) = 5.2 μ_B. Anal. for $C_{29}H_{44}FeN_4$ (calc.) C 69.04, H 8.79, N 11.10; (found) C 68.98, H 8.81, N 11.01.

5.2.6. *[(Me$_2$IPr)$_2$Fe](μ-κ-C,P-CH$_2$PMe$_2$)$_2$[Fe(κ-C,P-CH$_2$PMe$_2$)$_2$] (**4**)*

To a 25 mL flask charged with (Me$_2$IPr)FeCl$_2$ (277 mg, 0.902 mmol) and LiCH$_2$PMe$_2$ (148 mg, 1.80 mmol) was added via vacuum transfer 15 mL ether at −78 °C, resulting in an orange solution. The solution was allowed to warm slowly with stirring for 40 h. The volatiles were removed, and the orange residue taken up in 10 mL THF and filtered through dried Celite. Removal of the solvent, followed with washing the residue with hexanes (3 × 10 mL), resulted in an orange powder (285 mg, 82%). Crystals suitable for X-ray diffraction were obtained via layering a concentrated THF solution of **4** with pentane (1:3) and letting the solution stand at 23 °C for 12 h ^{1}H NMR (C_6D_6): δ 0.78 (2H), 2.31 (6H), 2.65 (6H), 5.42 (12H), 17.24 (6H), 27.15 (4H). μ_{eff} (Evans) = 5.0(3) μ_B.

5.2.7. *(PMe$_3$)$_2$Fe(κ-C,P-CH$_2$PMe$_2$)$_2$ (**5**)*

To a 25-mL flask charged with FeCl$_2$(PMe$_3$)$_2$ (340 mg, 1.22 mmol) and LiCH$_2$PMe$_2$ (200 mg, 2.44 mmol) was added 15 mL ether via vacuum transfer at −78 °C, resulting in a dark-brown solution. The solution was allowed to slowly warm to 23 °C for 2 d. The brown solution was filtered and the volatiles removed, producing a dark-brown residue. Attempts at trying to crystallize the compound from hexanes failed, as no solid precipitate was observed, regardless of concentration or temperature. The volatiles were evaporated, and the sticky brown solid was harvested (107 mg, 24%). ^{1}H NMR (C_6D_6): δ −1.81 (2H, s), −0.48 (2H, s), 1.17 (18H, "t", 3 Hz), 1.30 (6H, br s), 1.36 (6H, br s). ^{13}C NMR (C_6D_6): δ −6.98, 14.51, 16.66, 26.54. ^{31}P NMR (C_6D_6, ^{31}P coupling constants determined through spin simulation program MesReNova): δ −19.58, 30.06 (AA' = 27 Hz; XX' = 24 Hz, AX = A'X' = 61 Hz). Anal. for $C_{12}H_{34}FeP_4$ (calc.) C 40.24, H 9.57; (found) C 40.45, H 9.06.

5.2.8. *cis,trans-(PMe$_3$)$_2$Fe(κ-C,P-CH$_2$C$_6$H$_4$-o-PMe$_2$)$_2$ (**6**)*

A 60 mL bomb reactor was charged with CH$_3$C$_6$H$_4$-*o*-PMe$_2$ (250 mg, 1.63 mmol) and 15 mL benzene. A separate vial was charged with *cis*-Me$_2$Fe(PMe$_3$)$_4$ (319 mg, 0.817 mmol) and 3 mL benzene, and the it was added to the bomb, resulting in an orange solution. The solution was stirred for 1 d at 23 °C, followed by heating to 55 °C for 3 h. The volatiles were removed, and the solid residue was taken up in pentane/benzene and transferred to a separate 25 mL flask. The solvent was removed, and 10 mL pentane was added via vacuum transfer. The pentane mixture was cooled to −78 °C for 15 min, and filtered to afford a yellow powder (230 mg, 55%). ^{1}H NMR (C_6D_6): δ 0.87 (18H, d, 5 Hz), 1.40 (6H, t, 3 hz), 1.43 (6H, t, 2 Hz), 2.00 (2H, m), 2.39 (2H, dq, 15, 7 Hz), 7.03 (2H, t, 7 Hz), 7.10 (2H, t, 7 Hz), 7.23 (2H, dt, 7, 3 Hz), 7.43 (2H, d, 7 Hz). ^{13}C NMR (C_6D_6): δ 17.30 (t, 10 Hz), 20.10, 23.84 ("t", 8 Hz), 34.78 (t, 16 Hz), 123.18, 125.38, 128.59, 128.96 (t, 6 Hz), 145.40, 163.57 (t, 24 Hz). ^{31}P NMR (C_6D_6): δ 18.79 (t, 33 Hz), 53.50 (t, 33 Hz). Anal. for $C_{24}H_{42}FeP_4$ (calc.) C 56.48, H 8.30; (found) C 56.46, H 8.32.

5.3. NMR tube and small scale reactions

Flame-dried NMR tubes, sealed to 14/20 ground glass joints, were charged with metal reagent (typically ~10 mg, 10^{-2} mmol) and other solid substrates in the dry box, attached to needle valves, and moved to the vacuum line. The tubes were degassed, and after vacuum transfer of deuterated solvent, were flame sealed with a torch. In the case of small scale reactions, 10 mL or 25 mL flasks were loaded with reagents in the glovebox, and appended to needle valves. Solvents were added via vacuum transfer, and upon conclusion of the reaction, the volatiles were removed and the assembly transferred to the glovebox for analysis. Consult the text for particular reactions.

5.4. Single crystal X-Ray diffraction study

5.4.1. *Crystal data for **1***

$C_{36}H_{48}N_4Fe_2$, M = 648.48, monoclinic, $P2_1/c$, a = 9.8560 (7), b = 14.5425 (11), c = 12.4977 (9) Å, β = 111.796 (4)°, V = 1663 (9) Å^3, D = 1.295 g/cm^3, T = 223 (2) K, λ = 0.71073 Å, Z = 2, R_{int} = 0.0357, 16496 reflections, 3685 independent, R_1(all data) = 0.0480, wR_2 = 0.0994, GOF = 1.013, CCDC-1529975.

5.4.2. *Crystal data for **2***

$C_{84}H_{95}N_4LiP_3Fe$, M = 1316.33, triclinic, P-1, a = 13.2061 (6), b = 14.0219 (6), c = 20.7264 (10) Å, α = 98.823 (2)°, β = 101.703 (2)°, γ = 93.670 (2)°, V = 3695.8 (3) Å^3, D = 1.183 g/cm^3, T = 223 (2) K, λ = 0.71073 Å, Z = 2, R_{int} = 0.0468, 66905 reflections, 15088 independent, R_1(all data) = 0.0623, wR_2 = 0.0988, GOF = 1.025, CCDC-1529976.

5.4.3. *Crystal data for **4***

$C_{34}H_{72}N_4P_4Fe_2$, M = 772.53, monoclinic, $P2_1/n$, a = 13.1748 (6), b = 24.7344 (12), c = 13.3583 (7) Å, β = 91.399 (2)°, V = 4351.8 (4) Å^3, D = 1.179 g/cm^3, T = 223 (2) K, λ = 0.71073 Å, Z = 4, R_{int} = 0.0346, 39602 reflections, 8263 independent, R_1(all data) = 0.0463, wR_2 = 0.0821, GOF = 1.036, CCDC-1529977.

Acknowledgements

The authors thank the US National Science Foundation (CHE-1402149) and Cornell University for financial support.

Appendix A. Supplementary data

Supplementary data related to this article can be found at http://dx.doi.org/10.1016/j.jorganchem.2017.04.001.

References

[1] (a) R.R. Schrock, Angew. Chem. Int. Ed. 45 (2006) 3748–3759;
(b) R.R. Schrock, A.H. Hoveyda, Angew. Chem. Int. Ed. 42 (2003) 4592–4633.
[2] (a) R.H. Grubbs, Angew. Chem. Int. Ed. 45 (2006) 3760–3765;
(b) V.M. Marx, A.H. Sullivan, M. Melaimi, S.C. Virgil, B.K. Keitz, D.S. Weinberger, G. Bertrand, R.H. Grubbs, Angew. Chem. Int. Ed. 54 (2015)

1919–1923.
[3] Y. Chauvin, Angew. Chem. Int. Ed. 45 (2006) 3740–3747.
[4] O. Eisenstein, R. Hoffmann, A.R. Rossi, J. Am. Chem. Soc. 103 (1981) 5582–5584.
[5] B.M. Lindley, A. Swidan, E.B. Lobkovsky, P.T. Wolczanski, M. Adelhardt, J. Sutter, K. Meyer, Chem. Sci. 6 (2015) 4730–4736.
[6] B.M. Lindley, B.P. Jacobs, S.N. MacMillan, P.T. Wolczanski, Chem. Commun. 52 (2016) 3891–3894.
[7] B.P. Jacobs, R.G. Agarwal, P.T. Wolczanski, T.R. Cundari, S.N. MacMillan, Polyhedron 116 (2016) 47–56.
[8] P.T. Wolczanski, Organometallics 36 (2017) 622–631.
[9] L.E. Manzer, J. Am. Chem. Soc. 100 (1978) 8068–8073.
[10] (a) D.F. Evans, J. Chem. Soc. (1959) 2003–2005;
(b) E.M. Schubert, J. Chem. Ed. 69 (1992) 62.
[11] B.N. Figgis, M.A. Hitchman, Ligand Field Theory and its Applications, Wiley-VCH, New York, 2000.
[12] L.E. Manzer, L.J. Guggenberger, J. Organomet. Chem. 139 (1977) C34–C38.
[13] J.L. Latten, R.S. Dickson, G.B. Deacon, B.O. West, E.R.T. Tiekink, J.Organomet Chem. 435 (1992) 101–108.
[14] A.R. Hermes, G.S. Girolami, Organometallics 6 (1987) 763–768.
[15] R.B. Bedford, P.B. Brenner, E. Carter, P.M. Cogswell, M.F. Haddow, J.N. Harvey, D.M. Murphy, J. Nunn, C.H. Woodall, Angew. Chem. Int. Ed. 53 (2014) 1804–1808.
[16] L. Noël-Duchesneau, N. Lugan, G. Lavigne, A. Labande, V. César, Eur. J. Inorg. Chem. (2015) 1752–1758.
[17] S.J. Ryan, S.D. Schimler, D.C. Bland, M.S. Sanford, Org. Lett. 17 (2015) 1866–1869.
[18] (a) H. Zhang, Z. Ouyang, Y. Liu, Q. Zhang, L. Wang, L. Deng, Angew. Chem. Int. Ed. 53 (2014) 8432–8436;
(b) L. Wang, L. Hu, H. Zhang, H. Chen, L. Deng, J. Am. Chem. Soc. 137 (2015) 14196–14207;
(c) L. Zhang, Y. Liu, L. Deng, J. Am. Chem. Soc. 136 (2014) 15525–15528.
[19] (a) L. Xiang, J. Xiao, L. Deng, Organometallics 30 (2011) 2018–2025;
(b) Y. Liu, L. Wang, L. Deng, Organometallics 34 (2015) 4401–4407;
(c) Y. Liu, J. Xiao, L. Wang, Y. Song, L. Deng, Organometallics 34 (2015) 599–605;
(d) Y. Liu, L. Luo, J. Xiao, L. Wang, Y. Song, Y.J. Qu, Y. Luo, L. Deng, Inorg. Chem. 54 (2015) 4752–4760;
(e) Z. Mo, Z. Ouyang, L. Wang, K. Fillman, M.L. Neidig, L. Deng, Org. Chem. Front. 1 (2014) 1040–1044.
[20] (a) H.H. Karsch, H.-F. Klein, H. Schmidbaur, Chem. Ber. 110 (1977) 2200–2212;
(b) B. Blom, G. Tan, S. Enthaler, S. Inoue, J.D. Epping, M. Driess, J. Am. Chem. Soc. 135 (2013) 18108–18120.
[21] (a) K.W. Chiu, C.G. Howard, H.S. Rzepa, R.N. Sheppard, G. Wilkinson, A.M.R. Galas, M.B. Hursthouse, Polyhedron 1 (1982) 441–451;
(b) V.C. Gibson, P.D. Grebenik, M.L.H. Green, Chem. Comm. (1983) 1101–1102;
(c) V.C. Gibson, C.E. Graimann, P.M. Hare, M.L.H. Green, J.A. Bandy, P.D. Grebenik, K. Prout, J. Chem. Soc. Dalton Trans. (1985) 2025–2035;
(d) V.J. Murphey, G. Parkin, J. Am. Chem. Soc. 117 (1995) 3522–3528;
(e) D. Rabinovich, R. Zelman, G. Parkin, J. Am. Chem. Soc. 114 (1992) 4611–4621;
(f) A. Sattler, G. Parkin, J. Am. Chem. Soc. 133 (2011) 3748–3751;
(g) F.A. Cotton, J.A.M. Canich, R.L. Luck, K. Vidyasagar, Organometallics 10 (1991) 352–356;
(h) E.F. van Der Eide, W.E. Piers, M. Parvez, R. McDonald, Inorg. Chem. 46 (2007) 14–21;
(i) D.S. Kuiper, P.T. Wolczanski, E.B. Lobkovsky, T.R. Cundari, Inorg. Chem. 47 (2008) 10542–10553;
(j) R.T. Baker, J.C. Calabrese, R.L. Harlow, I.D. Williams, Organometallics 12 (1993) 830–841;
(k) Y. Jiao, W.W. Brennessel, W.D. Jones, Organometallics 34 (2015) 1552–1566;
(l) K.E. Janak, J.M. Tanski, D.G. Churchill, G. Parkin, J. Am. Chem. Soc. 124 (2002) 4182–4183;
(m) M. Sietzen, P. Federmann, C. Sonnenschein, H. Wadepohl, J. Ballmann, Dalton Trans. 45 (2016) 3013–3023.
[22] M.M. Meinholz, S.K. Pandey, S.M. Deuerlein, D. Stalke, Dalton Trans. 40 (2011) 1662–1671.
[23] H.H. Karsch, Chem. Ber. 110 (1977) 2222–2235.
[24] H.H. Karsch, Chem. Ber. 110 (1977) 2699–2711.
[25] E.R. Bartholomew, E.C. Volpe, P.T. Wolczanski, E.B. Lobkovsky, T.R. Cundari, J.Am. Chem. Soc. 135 (2013) 3511–3527.
[26] E.C. Volpe, P.T. Wolczanski, E.B. Lobkovsky, Organometallics 29 (2010) 364–377.
[27] (a) G. Xu, H. Sun, X. Li, Organometallics 28 (2009) 6090;
(b) X. Xu, J. Jia, H. Sun, Y. Liu, W. Xu, Y. Shi, D. Zhang, X. Li, Dalton Trans. 42 (2013) 3417.
[28] (a) R. Beck, T. Zheng, H. Sun, X. Li, U. Flörke, H.-F. Klein, J.Organomet Chem. 693 (2008) 3471;
(b) S. Camadanli, R. Beck, U. Flörke, H.-F. Klein, Organometallics 28 (2009) 2300;
(c) H.-F. Klein, S. Camadanli, R. Beck, D. Leukel, U. Flörke, Angew. Chem. Int. Ed. 44 (2005) 975;
(d) H.-F. Klein, S. Camadanli, R. Beck, U. Flörke, Chem. Commun. (2005) 381.
[29] J.T.B.H. Jastrzebski, G. van Koten, Inorg. Syn., Vol. 26, H. D. Kaesz, Ed., Inorganic Syntheses, Inc.: New York, 1089.
[30] S.A. Solomon, L.K. Allen, S.B.J. Dane, D.S. Wright, Eur. J. Inorg. Chem. (2014) 1615–1619.